Desalination and Water Treatment
www.deswater.com

doi: 10.5004/dwt.2022.27916

245 (2022) 92–105
January

Simultaneous anammox and denitrification process: start-up performance and mathematical simulation

Zhaozhao Wang[a,b], Xinjuan Wu[a,b], Huan Zhang[a,b], Peng Gao[c], Jun Ma[a,b], Chunyu Yin[a,b], Shuhao Zhu[a,b], Simin Li[a,b,*]

[a]*College of Energy and Environmental Engineering, Hebei University of Engineering, Handan 056038, China, Tel. +8617831917609; emails: 18303233729@163.com (S. Li), W-Z-Z@163.com (Z. Wang), wuxinjuan97@163.com (X. Wu), ZH982479127@163.com (H. Zhang), ma3590227@163.com (J. Ma), 13730039533@163.com (C. Yin)*
[b]*Center for Water Pollution Control and Water Ecological Remediation, Hebei University of Engineering, Handan 056038, China*
[c]*College of Architecture and Civil Engineering, Beijing University of Technology, Beijing 100124, China, email: 13082137058@163.com (P. Gao)*

Received 24 June 2021; Accepted 23 October 2021

ABSTRACT

The start-up performance of the simultaneous anammox and denitrification (SAD) process was studied in an upflow anaerobic sludge blanket (UASB) reactor with an effective volume of 10 L. The activity of heterotrophic denitrifying bacteria (DNB) increased when the C/N ratio was 0.25 over 53 d. Ammonia removal efficiency (ARE), chemical oxygen demand removal efficiency (CRE), nitrogen removal efficiency (NRE), and nitrogen removal rate (NRR) reached 93.27% ± 0.20%, 82.25% ± 0.04%, 82.39% ± 0.57% and 0.90 ± 0.02 kg/(m^3·d), respectively. A kinetic model of the biological reaction system of the SAD process start-up was developed based on the experimental data and a modified mathematical model (ASM1). The effectiveness of the model was verified based on the experimental data, and the nitrogen removal performance and changes in functional bacteria of the coupled system under different C/N ratios were investigated. The simulation revealed that the concentration and activity of anaerobic ammonia-oxidizing bacteria (AnAOB) gradually decreased, and DNB gradually increased, as the C/N ratio increased from 0.3 to 1.0. The optimal synergy of AnAOB and DNB and a stable NRE of 85.36% ± 0.48% were achieved when the C/N ratio was 0.6. Under this condition, the contributions of the anammox and denitrification processes to nitrogen removal ($E_{anammox}$ and $E_{denitrification}$) were 88.33% ± 0.23% and 11.67% ± 0.23%, respectively.

Keyword: Simultaneous anammox and denitrification; Nitrogen removal; C/N ratio; Functional bacteria; Mathematical simulation

1. Introduction

Nitrogen pollution by wastewater is becoming increasingly serious, and sewage discharge standards are becoming increasingly strict in China. There is thus an urgent need for research on efficient and stable biological nitrogen removal processes. The anammox process has attracted increased attention for its high efficiency and low cost. However, 7.5%–11% of total nitrogen (TN) is retained in the form of nitrate during the reaction process [1,2], which might prevent nitrate or TN discharge standards from being met. The simultaneous anammox and denitrification (SAD) process is highly efficient and cost-effective. Denitrifying bacteria use the organic matter (chemical oxygen demand: COD) in wastewater as an electron donor and reduce the by-products of anammox (NO_3^-–N) to N_2. Part of the NO_2^-–N

* Corresponding author.

1944-3994/1944-3986 © 2022 Desalination Publications. All rights reserved.

generated during the reaction also provides a substrate for the anammox reaction. Thus, the anammox coupled heterotrophic denitrification process can simultaneously remove nitrogen and organic matter in a single reactor. Zekker et al. [3] had improved the nitrogen and carbon removals in the anammox coupling with heterotrophic denitrification process at low temperature by switching the mainstream-sidestream wastewater. Moreover, this research team had successfully enhanced the nitrogen removal and electricity generation by coupling the anammox and heterotrophic denitrification processes in a microbial fuel cell system [4].

In the SAD process, the functional bacteria are extremely sensitive to the environment, and the cultivation period is long, both of which hinder the breadth of its application. Wang et al. [5] had successfully started up the SAD process by inducing the carbon source in to the anammox process and optimized the process by regulating the limited influent C/N ratios, which took 102 d in total. Similarly, this research team reported that it took 380 d and 81 d to successfully started up and optimize the simultaneous nitritation, anammox and denitrification (SNAD) process, respectively [6]. Thus, given that the cultivation time of functional bacteria is long in the start-up process, and experiments [7,8] have not been able to accurately reflect the operation of the coupling system under different C/N ratios, mathematical models have often been employed to assist in simulating and regulating sewage treatment systems. Compared with experiments, mathematical models are more time-efficient, require less labor, and are lower in cost. Consequently, SAD process start-up or optimization models and operational characteristics have become a major focus of research, and this work has provided insights into the start-up and optimization of the SAD process.

The ASM1 model is based on the Monod kinetic equation of the microbial growth, and the quantitative relationships within variables in the growth process are described by the stoichiometric coefficients so as to master the dynamics of the activated sludge process [9]. Few studies have been conducted on SAD process models. Bi et al. [10] established a SAD process model based on Activated Sludge Model No.3 (ASM3) and ASMN and used experimental data from batch experiments to calibrate the kinetic parameters. Comparison of the C/NO_3^-–N ratio and sludge concentration ratio (X_H/X_{AN}) revealed that the SAD process was optimized when C/NO_3^-–N was 1.5–2.0 and the sludge concentration ratio was 0.3–0.4. In addition, Yang et al. [11] used batch experiments to study the effect of organic matter (glucose and sodium acetate) on the SAD process. The experimental data and simulation results showed that the model could accurately simulate the nitrogen removal performance of the system, and there was no significant change in anaerobic ammonia-oxidizing bacteria (AnAOB) in the coupling system when the C/N ratio was in the range of 1–4. Azari et al. [12] established a model to study microbial community characteristics in the SAD process. The degradation of inorganic nitrogen under anoxic conditions was well explained after sensitivity analysis, calibration, and verification; microorganisms were also determined to have clear kinetic and physiological properties. Thus, exploration of mathematical models and operational characteristics is necessary for increasing the breadth of the applications of the SAD process.

It can be seen that previous SAD process models mainly focused on predictive results of carbon and nitrogen removals using sequencing batch reactors, whereas they rarely reported the simulation process of functional microflora dynamics in a continuous-flow SAD process. Thus, in this study, changes in nitrogen removal performance during the start-up period of the continuous-flow SAD process were analyzed. A mathematical model was then established based on these data using modified ASM1 to simulate and optimize the experimental process. Simulation results were verified, and the mathematical model was calibrated. In addition, the optimal C/N ratio of the continuous-flow SAD process was determined by investigating the nitrogen removal efficiency (NRE) and the change in functional bacteria of the SAD process in different running phases. The model output provides theoretical and predictive guidance that could be used to increase the efficiency of the continuous-flow SAD process for treating N-containing organic wastewater.

2. Materials and methods

2.1. Experimental setup and operation

The upflow anaerobic sludge blanket (UASB) reactor consisted of a sleeve-shaped plexiglass material with an effective volume of 10 L (Fig. 1A). The upper part of the reactor was equipped with a three-phase separator for the separation of the sludge, effluent, and gas. The outside of the reactor was covered with black material to preserve heat and block light. A water bath cycle was run with two heating rods submerged in the circulation tank to ensure that the temperature of the main reactor was constant. The reactor was equipped with an external reflux, and the rising velocity could be controlled by adjusting the speed of the reflux pump. The synthetic wastewater, together with the reflux flow, entered the bottom of the reactor, and the effluent flowed out from the upper outlet to the water tank.

2.2. Inoculated sludge and synthetic wastewater

2.2.1. Inoculated sludge and process performance

The inoculated sludge (anammox granular sludge) was obtained from a pilot-scale anammox-UASB reactor used for the treatment of high-nitrogen wastewater [5]. Before SAD process start-up, the anammox-UASB reactor had operated stably for three months treating synthetic wastewater containing ammonia and nitrite (NH_4^+–N: 149.91 ± 3.77 mg/L; NO_2^-–N: 196.36 ± 3.74 mg/L). The average NRE, nitrogen loading rate (NLR), and nitrogen removal rate (NRR) were 83.90% ± 2.01%, 1.42 ± 0.02 kg/(m^3·d), and 1.19 ± 0.03 kg/(m^3·d), respectively. The pH of the influent and effluent was approximately 7.8 ± 0.08 and 8.2 ± 0.15, respectively.

2.2.2. Synthetic wastewater and reactor operation

Synthetic wastewater was used as the substrate; the ammonia, nitrite, and organic matter originated from NH_4Cl, $NaNO_2$, and sodium acetate, respectively. The C/N ratio was defined as the COD/NO_x^-–N ratio in the influent;

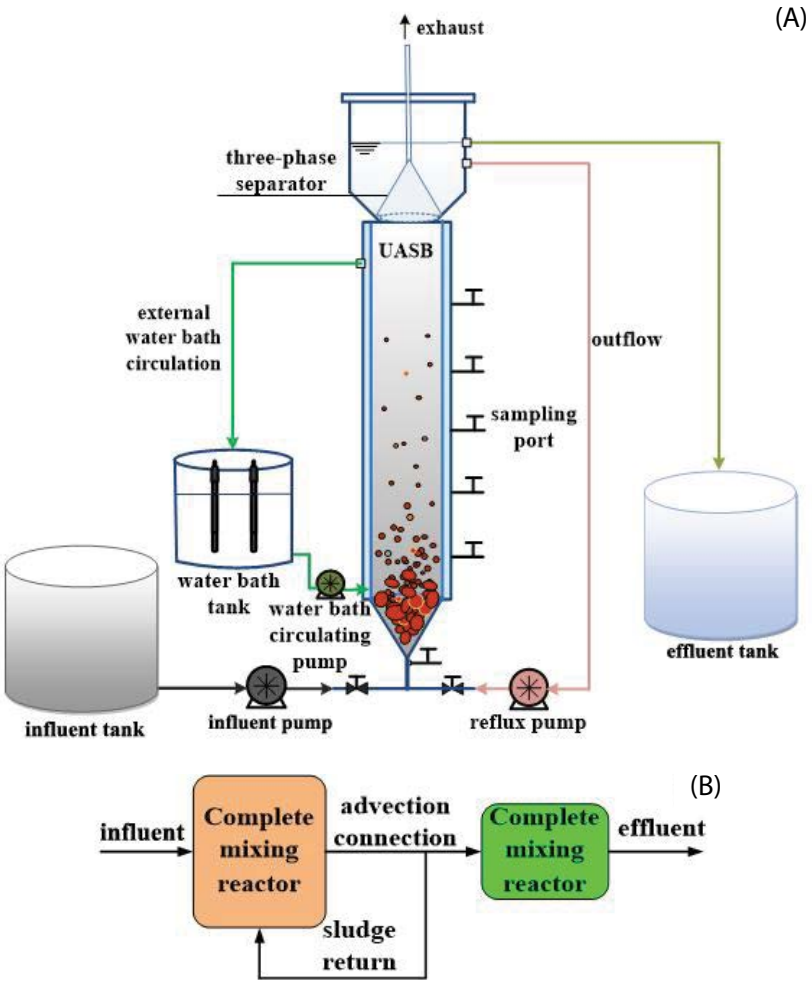

Fig. 1. Schematic diagram of the UASB reactor (A) and the simulated experimental device (B).

concentrations of nitrogen and organic matter varied among the experimental groups (Table 1). The other components and trace elements in the synthetic wastewater were as follows: 500 mg/L $NaHCO_3$; 27.2 mg/L KH_2PO_4; 180 mg/L $CaCl_2{\cdot}2H_2O$; and 300 mg/L $MgSO_4{\cdot}7H_2O$. Trace elements I and II were both supplied at 1 mL/L. The composition of trace element I was 1.25 g/L $KHCO_3$, 0.025 g/L KH_2PO_4, 0.3 g/L $CaCl_2{\cdot}2H_2O$, 0.2 g/L $MgSO_4{\cdot}7H_2O$, 0.00625 g/L $FeSO_4$, and that of trace element II was 15 g/L EDTA, 0.43 g/L $ZnSO_4{\cdot}7H_2O$, 0.24 g/L $CoCl_2{\cdot}6H_2O$, 0.99 g/L $MnCl_2{\cdot}4H_2O$, 0.25 g/L $CuSO_4{\cdot}5H_2O$, 0.22 g/L $NaMoO_4{\cdot}2H_2O$, 0.19 g/L $NiCl_2{\cdot}6H_2O$, 0.21 g/L $NaSeO_4{\cdot}10H_2O$, 0.014 g/L H_3BO_3, and 0.05 g/L $Na_2WO_4{\cdot}2H_2O$.

During operation, the hydraulic and environmental conditions of the reactor remained the same: the hydraulic retention time (HRT) was 8 h, the temperature was 33°C ± 1°C, and the influent pH range was 7.4–8.0.

2.3. Sample analyses and methods

Sampling was conducted every other day after filtration pre-treatment, and the samples were filtered through 0.45-μm filter paper. COD, NH_4^+–N, NO_2^-–N, NO_3^-–N, and mixed liquor suspended solids (MLSS) were measured according to standard methods [13], and the TN concentration was the sum of the NH_4^+–N, NO_2^-–N, and NO_3^-–N concentrations. Dissolved oxygen (DO), pH, and temperature values were monitored with a DO/pH sensor (Multi3630, WTW Co., Weilheim in Oberbayern, Germany).

The ammonia removal efficiency (ARE), NO_2^-–N removal efficiency, NRE, NLR, NRR, CRE, COD loading rate (CLR), COD removal rate (CRR), ΔNO_2^-–N/ΔNH_4^+–N ratio, ΔNO_3^-–N/ΔNH_4^+–N ratio, $E_{anammox}$, and $E_{denitrification}$ were calculated using the following formulas:

$$\mathrm{ARE} = \frac{NH_4^+ - N_{Inf} - NH_4^+ - N_{Eff}}{NH_4^+ - N_{Inf}} \quad (1)$$

$$NO_2^- - N \text{ removal efficiency} = \frac{NO_2^- - N_{Inf} - NO_2^- - N_{Eff}}{NO_2^- - N_{Inf}} \quad (2)$$

$$\mathrm{NRE} = \frac{TN_{Inf} - TN_{Eff}}{TN_{Inf}} \quad (3)$$

$$\mathrm{NLR} = \frac{TN_{Inf}}{HRT} \quad (4)$$

Table 1
Composition of the influent in the SAD process during the start-up and optimization periods

Period	Operation time (d)	NH_4^+–N (mg/L)	NO_2^-N (mg/L)	NO_3^-N (mg/L)	COD (mg/L)	C/N ratio
Start-up	1~53	149.91 ± 3.77	196.36 ± 3.74	9.77 ± 1.04	50.97 ± 1.89	0.25
Optimization	54~74	149.46 ± 4.78	198.69 ± 7.24	10.21 ± 1.17	82.55 ± 2.57	0.4
	75~97	149.47 ± 3.15	198.54 ± 5.58	10.63 ± 1.10	123.26 ± 3.53	0.6
	98~110	150.11 ± 1.93	198.21 ± 6.89	10.01 ± 0.88	165.62 ± 3.39	0.8
	111~121	148.26 ± 5.43	198.27 ± 2.01	10.10 ± 1.17	208.54 ± 3.56	1.0

Note: Concentrations in the table correspond to the average values of the actual influent concentration.

$$NRR = \frac{\left(TN_{Inf} - TN_{Eff}\right)}{HRT} \quad (5)$$

$$CRE = \frac{COD_{Inf} - COD_{Eff}}{COD_{Inf}} \quad (6)$$

$$CLR = \frac{COD_{Inf}}{HRT} \quad (7)$$

$$CRR = \frac{\left(COD_{Inf} - COD_{Eff}\right)}{HRT} \quad (8)$$

$$\Delta NO_2^- - N/\Delta NH_4^+ - N = \frac{NO_2^- - N_{Inf} - NO_2^- - N_{Eff}}{NH_4^+ - N_{Inf} - NH_4^+ - N_{Eff}} \quad (9)$$

$$\Delta NO_3^- - N/\Delta NH_4^+ - N = \frac{NO_3^- - N_{Inf} - NO_3^- - N_{Eff}}{NH_4^+ - N_{Inf} - NH_4^+ - N_{Eff}} \quad (10)$$

$$E_{anammox} = \frac{\Delta NH_4^+ - N + 1.32\Delta NH_4^+ - N - 0.26\Delta NH_4^+ - N}{\Delta NH_4^+ - N + \Delta NO_2^- - N - \Delta NO_3^- - N} \times 100\% \quad (11)$$

$$E_{denitrification} = 100\% - E_{anammox} \quad (12)$$

2.4. Mathematical model

2.4.1. Model selection

The Activated Sludge Model No.1 (ASM1) is often used to develop other models and is central to other coupling models and modified models. ASM1 is a model of the biological reaction process based on Monod equations. The relationships within the variables and the relevant constants of this model are characterized by the stoichiometric matrix to simulate the biological reaction processes. In this paper, a UASB reactor was used for the SAD process. The modified ASM1 model was finally established by inducing the bioreaction, constituents, and parameters of the anammox process into the ASM1 using AQUASIM 2.0 software [6], which could simulate the biochemical reactions occurring in the reactor and was therefore suitable for this research. The application of this model can intuitively show changes in substrate concentration, functional bacteria concentration, and substrate degradation rate.

This model involves four functional microbial species: aerobic ammonia-oxidizing bacteria (AerAOB), nitrite-oxidizing bacteria (NOB), anammox bacteria (AnAOB), and heterotrophic denitrifying bacteria (DNB). Thirteen constituents, 11 process kinetics, and the stoichiometric matrix used for the model are shown in Table 2; 11 process kinetic rate equations for this model are shown in Table 3; the kinetics and stoichiometric parameters of this model are shown in Table 4; and the formulas for calculating the conversion rates of oxygen, ammonia, nitrite, and nitrate by different microbial species are shown in Table 5.

2.4.2. Model construction and calibration

In this model, an experimental device with two serial-connected completely mixed reactors was used, and the sludge recirculation flow was 100%. The specific schematic diagram of the process is shown in Fig. 1B. The mathematical model of the SAD process was established using the experimental data and AQUASIM 2.0 software; the sensitivity of the model parameters was also analyzed using this software (specifically, the influence of the selected parameter on the model simulation value was analyzed through the preliminary pre-calculation of the designed model). The model parameters were corrected according to the results of the sensitivity analysis (Table 6).

3. Results and discussion

3.1. SAD process start-up performance analysis

The start-up of the SAD process was initiated by the addition of an organic carbon source (sodium acetate) to the feed water based on the anammox process. To achieve the coupling of AnAOB and DNB, the SAD process was operated under a C/N ratio of 0.25 for 53 d.

During the start-up of the SAD process, the average influent concentrations of NH_4^+–N, NO_2^-–N, NO_3^-–N, and COD were 149.91 ± 3.77 mg/L, 196.36 ± 3.74 mg/L, 9.77 ± 1.04 mg/L, and 50.97 ± 1.89 mg/L, respectively (Fig. 2). On the first day, the effluent concentrations of NH_4^+–N, NO_2^-–N, and TN increased from 6.61, 20.05, and 71.85 mg/L to 19.94, 24.04, and 89.17 mg/L, respectively. The removal efficiencies decreased from 95.37%, 90.18%, and 79.85% to 86.31%, 87.73%, and 74.54%, respectively. The reason for this decline in performance might stem from the high sensitivity of AnAOB to the environment. The addition of sodium acetate made the environmental conditions,

Table 2
Stoichiometric matrix for the model

Process \ Variable	S_{O_2}	S_S	S_{NH_4}	S_{NO_2}	S_{NO_3}	S_{N_2}	S_I	X_S	X_{AOB}	X_{NOB}	X_{AN}	X_H	X_I
	O_2	COD	N	N	N	N	COD	COD	COD	COD	COD	COD	COD
1	$-(3.43-Y_{AOB})/Y_{AOB}$		$-i_{NBM}-1/Y_{AOB}$	$1/Y_{AOB}$					1				
2								$1-f_I$	–1				f_I
3	$-(1.14-Y_{NOB})/Y_{NOB}$		$-i_{NBM}$	$-1/Y_{NOB}$	$1/Y_{NOB}$					1			
4								$1-f_I$		–1			f_I
5			$-i_{NBM}-1/Y_{AN}$	$-1/Y_{AN}-1/1.14$	1/1.14	$2/Y_{AN}$					1		
6								$1-f_I$			–1		f_I
7		0.9	i_{NBM}				0.1	–1					
8	$-(1-Y_H)/Y_H$	$-1/Y_H$	$-i_{NBM}$									1	
9		$-1/Y_H$	$-i_{NBM}$	$-(1-Y_H)/1.72/Y_H$		$(1-Y_H)/1.72/Y_H$						1	
10		$-1/Y_H$	$-i_{NBM}$	$(1-Y_H)/1.14/Y_H$	$-(1-Y_H)/1.14/Y_H$							1	
11								$1-f_I$				–1	f_I

Table 3
Process kinetic rate equations for the model

Process	Kinetics rates expressions
Growth of AOB	$\mu_{AOB}\frac{S_{O_2}}{K_{O_2}^{AOB}+S_{O_2}}\frac{S_{NH_4}}{K_{NH_4}^{AOB}+S_{NH_4}}X_{AOB}$
AOB decay	$b_{AOB}X_{AOB}$
Growth of NOB	$\mu_{NOB}\frac{S_{O_2}}{K_{O_2}^{NOB}+S_{O_2}}\frac{S_{NO_2}}{K_{NO_2}^{NOB}+S_{NO_2}}X_{NOB}$
NOB decay	$b_{NOB}X_{NOB}$
Growth of AnAOB	$\mu_{AN}\frac{K_{O_2}^{AN}}{K_{O_2}^{AN}+S_{O_2}}\frac{S_{NH_4}}{K_{NH_4}^{AN}+S_{NH_4}}\frac{S_{NO_2}}{K_{NO_2}^{AN}+S_{NO_2}}X_{AN}$
AnAOB decay	$b_{AN}X_{AN}$
Hydrolysis	$k_H\frac{X_S/X_H}{K_X+X_S/X_H}X_H$
Aerobic growth of X_H	$\mu_H\frac{S_{O_2}}{K_{O_2}^{H}+S_{O_2}}\frac{S_S}{K_S+S_S}X_H$
Anoxic growth of X_H using nitrite	$\mu_H\eta_{H,NO_2}\frac{K_{O_2}^{H}}{K_{O_2}^{H}+S_{O_2}}\frac{S_{NO_2}}{K_{NO_2}^{H}+S_{NO_2}}\frac{S_S}{K_S+S_S}X_H$
Anoxic growth of X_H using nitrate	$\mu_H\eta_{H,NO_3}\frac{K_{O_2}^{H}}{K_{O_2}^{H}+S_{O_2}}\frac{S_{NO_3}}{K_{NO_3}^{H}+S_{NO_3}}\frac{S_S}{K_S+S_S}X_H$
X_H decay	b_HX_H

less suitable for AnAOB growth, which affected AnAOB activity and reduced nitrogen removal performance.

As the reaction progressed, AnAOB began to adapt to the organic environment. After 52 d of operation, the effluent NH_4^+–N and NO_2^-–N concentrations decreased to 10.18 and 16.38 mg/L, respectively, on day 53 (Fig. 2A). The removal efficiencies increased to 93.43% and 91.79%, respectively, and the removal loads were stabilized at 0.43 and 0.60 kg/(m^3·d), respectively, indicating that the addition of sodium acetate did not permanently inhibit AnAOB. After a period of adaptation, AnAOB activity recovered and increased; the effluent NO_3^-–N concentration gradually decreased from 45.19 to 35.22 mg/L. The anammox reaction involved the reaction of NH_4^+–N and NO_2^-–N to form NO_3^-–N, whereas heterotrophic denitrification involved the activity of DNB on NO_2^-–N or NO_3^-–N as electron acceptor, resulting in the generation of N_2. The effluent NH_4^+–N and NO_2^-–N concentrations all decreased, indicating that the addition of sodium acetate had no obvious inhibitory effect on the anammox reaction and that it proceeded normally; the effluent NO_3^-–N concentration decreased, which indicated that the low carbon concentration promoted DNB growth and activity, permitted DNB to consume NO_3^-–N, and reduced the effluent NO_3^-–N concentration. This suggested that both anammox and heterotrophic denitrification reactions were occurring in the

Table 4
Kinetic and stoichiometric parameters of the model

Parameter	Definition	Values	Unit	Source
	Aerobic ammonium oxidizing bacteria (AOB)			
Y_{AOB}	Yield coefficient for AOB	0.15	g COD g^{-1} N	[17]
μ_{AOB}	Maximum growth rate of AOB	0.054	h^{-1}	[18]
b_{AOB}	Decay rate coefficient of AOB	0.0054	h^{-1}	[17]
$K_{O_2}^{AOB}$	S_{O_2} affinity constant for AOB	0.5	g DO m^{-3}	[17]
$K_{NH_4}^{AOB}$	S_{NH_4} affinity constant for AOB	2.4	g N m^{-3}	[17]
	Nitrite oxidizing bacteria (NOB)			
Y_{NOB}	Yield coefficient for NOB	0.041	g COD g^{-1} N	[17]
μ_{NOB}	Maximum growth rate of NOB	0.061	h^{-1}	[18]
b_{NOB}	Decay rate coefficient of NOB	0.0025	h^{-1}	[17]
$K_{O_2}^{NOB}$	S_{O_2} affinity constant for NOB	0.68	g DO m^{-3}	[17]
$K_{NO_2}^{NOB}$	S_{NO_2} affinity constant for NOB	5.5	g N m^{-3}	[19]
	Anaerobic ammonium oxidizing bacteria (AnAOB)			
Y_{AN}	Yield coefficient for AnAOB	0.159	g COD g^{-1} N	[20]
μ_{AN}	Maximum growth rate of AnAOB	0.0041	h^{-1}	[18]
b_{AN}	Decay rate coefficient of AnAOB	0.00013	h^{-1}	[21]
$K_{O_2}^{AN}$	S_{O_2} inhibiting coefficient for AnAOB	0.01	g DO m^{-3}	[21]
$K_{NH_4}^{AN}$	S_{NH_4} affinity constant for AnAOB	0.07	g N m^{-3}	[22]
$K_{NO_2}^{AN}$	S_{NO_2} affinity constant for AnAOB	0.05	g N m^{-3}	[21]
	Heterotrophic bacteria (H)			
Y_H	Aerobic yield coefficient for X_H	0.54	g COD g^{-1} COD	[22]
μ_H	Maximum growth rate of X_H	0.3	h^{-1}	[18]
b_H	Decay rate coefficient of X_H	0.0083	h^{-1}	[17]
k_H	Hydrolysis rate constant	0.125	h^{-1}	[22]
K_X	Hydrolysis saturation constant	1	g COD g^{-1} COD	[22]
$K_{O_2}^{H}$	S_{O_2} inhibiting coefficient for X_H	0.2	g DO m^{-3}	[22]
K_S	S_S affinity constant for X_H	10	g COD m^{-3}	[22]
$K_{NO_2}^{H}$	S_{NO_2} affinity constant for X_H	0.5	g N m^{-3}	[21]
$K_{NO_3}^{H}$	S_{NO_3} affinity constant for X_H	0.5	g N m^{-3}	[22]
η_{H,NO_2}	Reduction factor for denitrification NO_2–N_2	0.25	–	[23]
η_{H,NO_3}	Reduction factor for denitrification NO_3–NO_2	0.15	–	[23]
	Other stoichiometric parameters			
i_{NBM}	Nitrogen content of biomass	0.07	g N g^{-1} COD	[24]
i_{NXI}	Nitrogen content of X_I	0.02	g N g^{-1} COD	[24]
f_I	Fraction of X_I in biomass decay	0.10	g COD g^{-1} COD	[24]

reactor, and the anammox-generated NO_3^-–N was removed via the heterotrophic denitrification process.

NRE increased from 74.54% to 82.99% and stabilized at around 81.38% ± 0.80% (Fig. 2B). The NLR and NRR reached 1.09 kg/(m^3·d) and 0.90 kg/(m^3·d), respectively. The addition of organic matter had no long-term inhibitory effect on the anammox reaction, and after a period of adaptation, the AnAOB activity increased. The NRE of the coupling system

Table 5
Formulas for calculating the conversion rates of oxygen, ammonia, nitrite and nitrate by different microbial species

Description	Formulas
Oxygen uptake rate by AOB	$-\left(1-\frac{3.43}{Y_{AOB}}\right)\mu_{AOB}\frac{S_{O_2}}{K_{O_2}^{AOB}+S_{O_2}}\frac{S_{NH_4}}{K_{NH_4}^{AB}+S_{NH_4}}X_{AOB}$
Oxygen uptake rate by NOB	$-\left(1-\frac{1.14}{Y_{NOB}}\right)\mu_{NOB}\frac{S_{O_2}}{K_{O_2}^{NOB}+S_{O_2}}\frac{S_{NO_2}}{K_{NO_2}^{NO}+S_{NO_2}}X_{NOB}$
Oxygen uptake rate by heterotrophic bacteria	$-\left(1-\frac{1}{Y_H}\right)\mu_H\frac{S_{O_2}}{K_{O_2}^{H}+S_{O_2}}\frac{S_S}{K_S+S_S}X_H$
Ammonium uptake rate by AOB	$-\left(-i_{NBM}-\frac{1}{Y_{AN}}\right)\mu_{AOB}\frac{S_{O_2}}{K_{O_2}^{AOB}+S_{O_2}}\frac{S_{NH_4}}{K_{NH_4}^{AOB}+S_{NH_4}}X_{AOB}$
Ammonium uptake rate by AnAOB	$-\left(-i_{NBM}-\frac{1}{Y_{AN}}\right)\mu_{AN}\frac{K_{O_2}^{AN}}{K_{O_2}^{AN}+S_{O_2}}\frac{S_{NH_4}}{K_{NH_4}^{AN}+S_{NH_4}}\frac{S_{NO_2}}{K_{NO_2}^{AN}+S_{NO_2}}X_{AN}$
Nitrite uptake rate by NOB	$\frac{1}{Y_{NOB}}\mu_{NOB}\frac{S_{O_2}}{K_{O_2}^{NOB}+S_{O_2}}\frac{S_{NO_2}}{K_{NO_2}^{NO}+S_{NO_2}}X_{NOB}$
Nitrite uptake rate by AnAOB	$-\left(-\frac{1}{Y_{AN}}-\frac{1}{1.14}\right)\mu_{AN}\frac{K_{O_2}^{AN}}{K_{O_2}^{AN}+S_{O_2}}\frac{S_{NH_4}}{K_{NH_4}^{AN}+S_{NH_4}}\frac{S_{NO_2}}{K_{NO_2}^{AN}+S_{NO_2}}X_{AN}$
Nitrite uptake rate by denitrifiers	$\frac{\left(1-Y_H\times 0.8\right)}{1.72/\left(Y_H\times 0.8\right)}\mu_H\eta_{H,NO_2}\frac{K_{O_2}^{H}}{K_{O_2}^{H}+S_{O_2}}\frac{S_{NO_2}}{K_{NO_2}^{H}+S_{NO_2}}\frac{S_S}{K_S+S_S}X_H$
Nitrate uptake rate by denitrifiers	$\frac{\left(1-Y_H\times 0.8\right)}{1.14/\left(Y_H\times 0.8\right)}\mu_H\eta_{H,NO_2}\frac{K_{O_2}^{H}}{K_{O_2}^{H}+S_{O_2}}\frac{S_{NO_2}}{K_{NO_2}^{H}+S_{NO_2}}\frac{S_S}{K_S+S_S}X_H$
Nitrate production rate by AnAOB	$\frac{1}{1.14}\mu_{AN}\frac{K_{ON}^{AN}}{K_{O_2}^{AN}+S_{O_2}}\frac{S_{NH_4}}{K_{NH_4}^{AN}+S_{NH}}\frac{S_{NO_2}}{K_{NO_2}^{AN}+S_{NO_2}}X_{AN}$

was 3.14% higher than that of the anammox system alone, which indicated that AnAOB and DNB achieved high synergistic nitrogen removal in this experiment. The coupling of anammox and heterotrophic denitrification increased the NRE and mediated the start-up of the SAD process.

During the SAD start-up process, the influent COD stabilized at about 50.97 ± 1.89 mg/L, and the effluent COD concentration decreased from 12.57 to 9.47 mg/L during the first 23 d and then stabilized at about 9.15 mg/L (Fig. 2C). The removal efficiency increased from 73.60% to 80.91% from day 1 to day 23 and then stabilized at around 82.21% ± 1.30%. CLR and CRR stabilized at around 0.15 ± 0.01 kg/(m^3·d) and 0.13 ± 0.01 kg/(m^3·d), respectively. The gradual decrease in the effluent concentration and the gradual increase in the removal rate indicated that COD participated in the denitrification reaction and was consumed by DNB, which is the result of increased heterotrophic denitrification.

$E_{anammox}$ on day 1 was 99.17% and decreased during the start of the SAD process. By day 53, the NRE decreased to 93.81%. By contrast, $E_{denitrification}$ increased from 0.83% to 6.19% during the experimental period, which was attributed to the growth and enhanced activity of DNB. However, the anammox process was still the dominant pathway in the coupling system. This stemmed from the fact that the organic carbon concentration was low when the C/N ratio was 0.25, which restricted the growth of DNB. Furthermore, the results indicate that DNB did not compete with AnAOB for NO_2^-–N but used the NO_3^-–N produced during the anammox process, which can be explained by the variations in the stoichiometric ratio (Fig. 2D). Specifically, the ratio of ΔNO_2^-–N/ΔNH_4^+–N did not change significantly during the start-up of the SAD process and remained around 1.32 ± 0.03. The ratio of ΔNO_3^-–N/ΔNH_4^+–N decreased during the first 17 days from 0.29 to 0.19 and remained stable around 0.19 ± 0.03, which was lower than the theoretical value of 0.26. These results were consistent with Song et al [14]. The effluent pH fluctuated between 7.86–8.41, which was higher than the pH of the

Table 6
Model parameter estimation results

Parameter	Definition	Values	Unit
μ_{AOB}	Maximum growth rate of AOB	1.2019948	d^{-1}
b_{AOB}	Decay rate coefficient of AOB	0.053524856	d^{-1}
$K_{O_2}^{AOB}$	S_{O_2} affinity constant for AOB	2.4362372	g DO m^{-3}
$K_{NH_4}^{AOB}$	S_{NH_4} affinity constant for AOB	6.6228145	g N m^{-3}
μ_{NOB}	maximum growth rate of NOB	1.417238	d^{-1}
b_{NOB}	decay rate coefficient of NOB	0.099957958	d^{-1}
$K_{O_2}^{NOB}$	S_{O_2} affinity constant for NOB	1.5024107	g DO m^{-3}
$K_{NO_2}^{NOB}$	S_{NO_2} affinity constant for NOB	9.9709254	g N m^{-3}
μ_{AN}	maximum growth rate of anammox	0.045108297	d^{-1}
b_{AN}	decay rate coefficient of anammox	0.0094132309	d^{-1}
$K_{O_2}^{AN}$	S_{O_2} inhibiting coefficient for anammox	5.337681	g DO m^{-3}
$K_{NH_4}^{AN}$	S_{NH_4} affinity constant for anammox	9.6944575	g N m^{-3}
$K_{NO_2}^{AN}$	S_{NO_2} affinity constant for anammox	8.658779	g N m^{-3}
μ_H	maximum growth rate of X_H	2.777668	d^{-1}
b_H	decay rate coefficient of X_H	4.4780147	d^{-1}
k_H	Hydrolysis rate constant	4.5388006	d^{-1}
K_X	Hydrolysis saturation constant	4.5702648	g COD g^{-1} COD
$K_{O_2}^{H}$	S_{O_2} inhibiting coefficient for X_H	0.89118629	g DO m^{-3}
K_S	S_S affinity constant for X_H	5.7743722	g COD m^{-3}
$K_{NO_2}^{H}$	S_{NO_2} affinity constant for X_H	0.82415142	g N m^{-3}
$K_{NO_3}^{H}$	S_{NO_3} affinity constant for X_H	9.1555851	g N m^{-3}
η_{H,NO_2}	reduction factor for denitrification NO_2–N_2	2.8803855	–
η_{H,NO_3}	reduction factor for denitrification NO_3–NO_2	0.31480395	–

influent (7.43–7.71). This can be explained by the fact that the anammox and denitrification processes are alkali-generating bioreactions, and the SAD process could achieve water productions at higher pH.

Overall, adding a small amount of organic carbon into the anammox system could help induce DNB in the system and improve the nitrogen and carbon removal performances, which results in a stronger coupling of anammox and denitrification and facilitates the completion of SAD process start-up.

3.2. Mathematical model and simulation of SAD process start-up

After conducting the experiments described above on the nitrogen removal performance of SAD process start-up, a preliminary SAD process start-up model was established based on the experimental data. The goal of this work was to simulate changes in functional bacteria during SAD process start-up and provide technology to support C/N ratio optimization of the SAD process.

3.2.1. Mathematical simulation and experimental verification

Simulations were performed to determine the effluent values of NH_4^+–N, NO_2^-–N, NO_3^-–N, and COD during the SAD process. Actual experimental data were employed for the verification (Fig. 3).

The simulated effluent values during the start-up period of the SAD process were consistent with the actual effluent values (Fig. 3A). The actual effluent of NH_4^+–N was reduced from 19.94 to 10.58 mg/L, and the simulated value was reduced from 19.94 to 11.48 mg/L. The actual effluent values of NH_4^+–N were greater than the simulated ones during the first 17 d of operation. This can be explained by the fact that after the addition of the carbon source, the AnAOB did not rapidly adapt to the organic environment; thus, ammonia biodegradation via the anammox process was inhibited [15]. As the reactor continued to operate, the experimental effluent concentration of NH_4^+–N decreased, and the actual value ended up being close to the simulated value. The actual effluent values of NO_2^-–N, NO_3^-–N, and COD decreased from 24.04, 45.19, and 12.57 mg/L to 16.38,

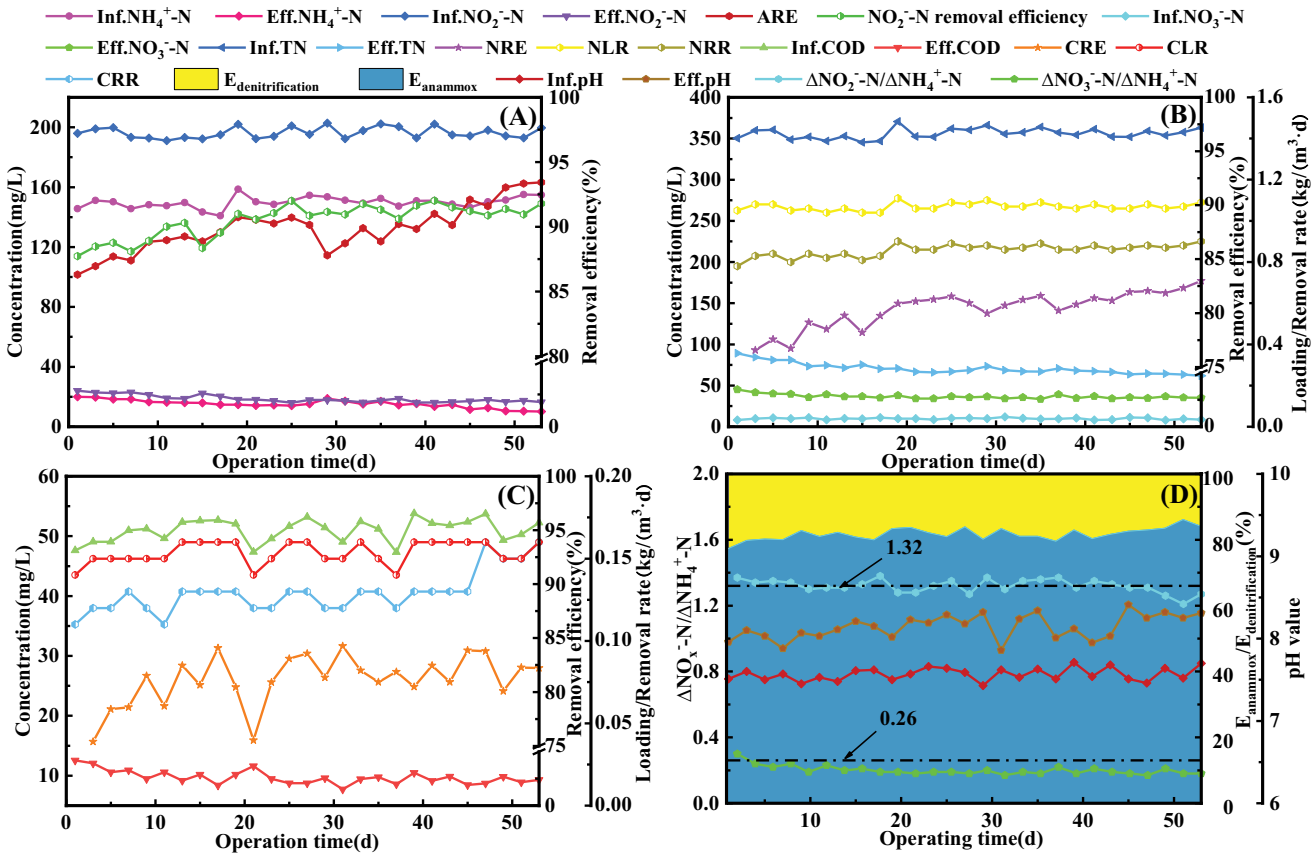

Fig. 2. Performance during the start-up period of the SAD process. (A) Ammonia and nitrite removal, (B) nitrate and TN removal, (C) COD removal, and (D) changes in $E_{anammox}$, $E_{denitrification}$, ΔNO_x^-–N/ΔNH_4^+–N ratios, and pH.

35.22, and 9.29 mg/L, respectively. The corresponding simulated effluent values showed similar consistent decreases from 24.04, 45.19, and 12.57 mg/L to 14.85, 35.75, and 9.42 mg/L, respectively.

The NRE, NRR, CRE, and CRR were also simulated based on the effluent simulation values during the SAD start-up process (Fig. 3B). The experimental values of NRE, NRR, CRE, and CRR were close to the simulated ones, and the trends were consistent. The experimental values of NRE and NRR increased from 74.54% and 0.78 kg/(m^3·d) to 82.99% and 0.90 kg/(m^3·d), respectively, and their simulated ones increased from 74.54% and 0.78 kg/(m^3·d) to 82.90% and 0.90 kg/(m^3·d), respectively. The experimental values of CRE and CRR increased from 73.60% and 0.11 kg/(m^3·d) to 82.22% and 0.16 kg/(m^3·d), respectively, whereas the simulated ones increased from 73.60% and 0.12 kg/(m^3·d) to 81.98% and 0.16 kg/(m^3·d) respectively. These results indicated that the simulation of this mathematical model was consistent with the experimental values.

Overall, the simulation of the SAD start-up process performed well compared with the experimental values. The simulation values were generally close to the experimental ones; similar trends were observed, and the degree of consistency was high (Fig. 3). This indicated that the mathematical model could accurately reflect the bioreactions of the SAD process during the entire experiment. This model facilitates subsequent analyses of the concentration and activity of functional bacteria during this period and can be used to optimize the SAD process.

3.2.2. Changes in the concentration and activity of functional bacteria during SAD process start-up

The validated SAD process start-up model was used to analyze the concentration and activity of functional bacteria (Fig. 4A). Overall, four main functional bacterial groups were observed in the SAD process: AerAOB, NOB, AnAOB, and DNB. AnAOB was the dominant group and facilitated the anammox reaction; its concentration increased from 2,949.00 mg MLSS/L to 4,447.00 mg MLSS/L after the SAD start-up process. Similar to AnAOB, the DNB concentration also increased because of the addition of an organic carbon source (from 10.36 mg MLSS/L to 28.46 mg MLSS/L). However, because of the limited concentration of organic matter added, the growth of DNB was relatively slow, which also provided sufficient space to support the growth of AnAOB [16]. Concentrations of AerAOB and NOB were lower than those of AnAOB and DNB, which was beneficial for the SAD process. AOB abundance changed little and remained close to zero. However, the abundance of NOB increased from 8.67 mg MLSS/L to 13.19 mg MLSS/L, which stemmed the

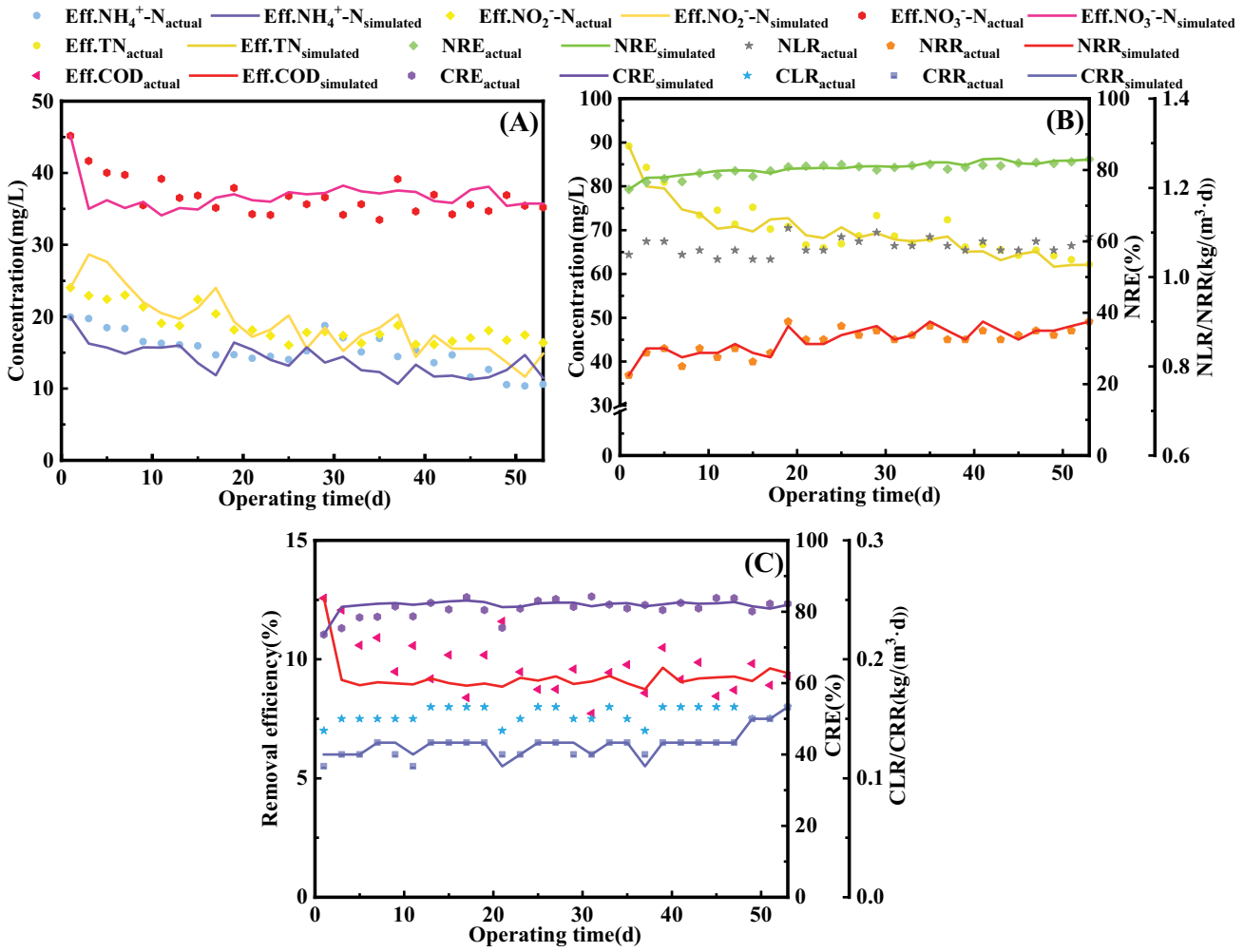

Fig. 3. The performance and simulation results of the SAD process during the start-up period. (A) NH_4^+–N, NO_2^-–N, and NO_3^-–N removal, (B) TN removal, and (C) COD removal.

small amount of dissolved oxygen in the feed water to the reactor.

In addition, substrate degradation rates were determined to further characterize AnAOB and DNB activity (Fig. 4B). The degradation rates of NH_4^+–N and NO_2^-–N by AnAOB increased from 0.403 and 0.455 kg N/(m^3 d) to 0.421 and 0.475 kg N/(m^3 d), respectively. The degradation rate of NO_2^-–N and NO_3^-–N by DNB increased from 0.001 and 0.006 kg N/(m^3 d) to 0.003 and 0.016 kg N/(m^3 d), respectively, which stemmed from the growth of DNB driven by the addition of an organic carbon source in the system.

3.3. SAD process performance optimization

3.3.1. Influence of different C/N ratios on SAD process performance

3.3.1.1. Model simulation of SAD process performance under different C/N ratios

Based on the calibration and verification of the SAD process start-up model, the influent substrate concentrations were set and substituted into the model to simulate the effluent concentrations at different C/N ratios; the removal performance was then calculated.

The simulated influent concentrations of NH_4^+–N, NO_2^-–N, and NO_3^-–N were 150.0, 198.0, and 9.8 mg/L, respectively. The simulated COD influent concentrations were set based on the different C/N ratios. The set reaction time was 31 d, as the process performance at each C/N ratio could only reach a stable state after a long period, and the other reaction conditions remained the same. The simulated effluent concentration and removal efficiency of each substrate at each C/N ratio through the mathematical model are shown in Table 7.

When the C/N ratio increased from 0.3 to 1.0, the simulated effluent NH_4^+–N concentration gradually increased from 10.67 to 36.69 mg/L, and the ARE gradually decreased from 92.89% to 75.54%. As the C/N ratio increased, the DNB could use the organic carbon source for growth and reproduction, and the activity of AnAOB was inhibited and reduced, thereby affecting the efficiency of the anammox reaction. As the ARE gradually decreased, the simulated

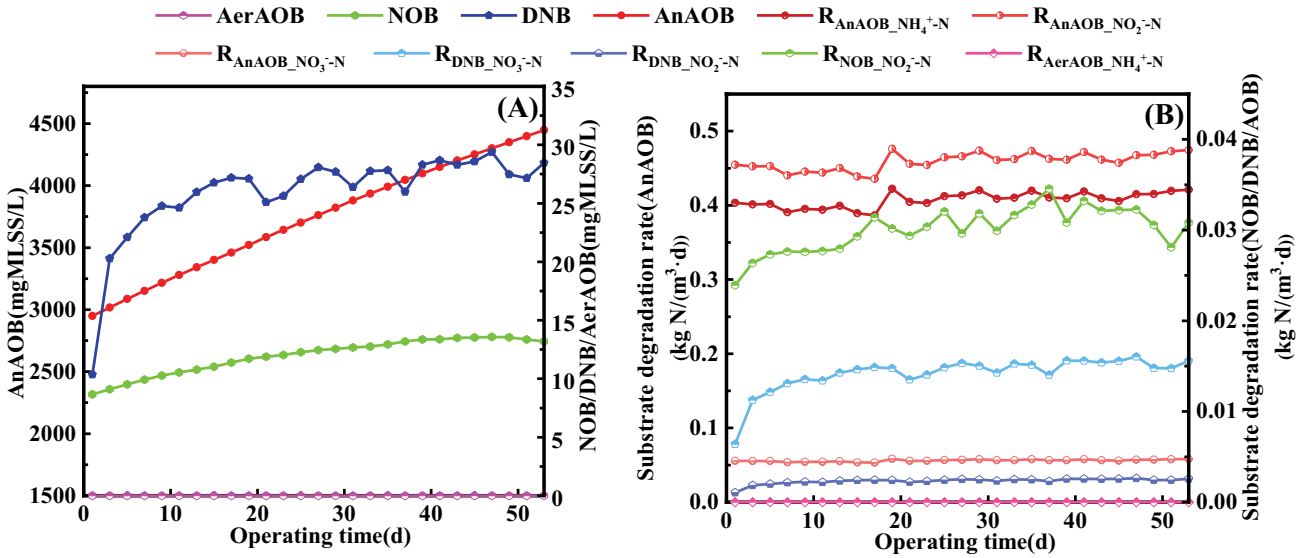

Fig. 4. Simulation of the concentrations (A) and activities (B) of the functional bacteria at different C/N ratios during the start-up period of the SAD process.

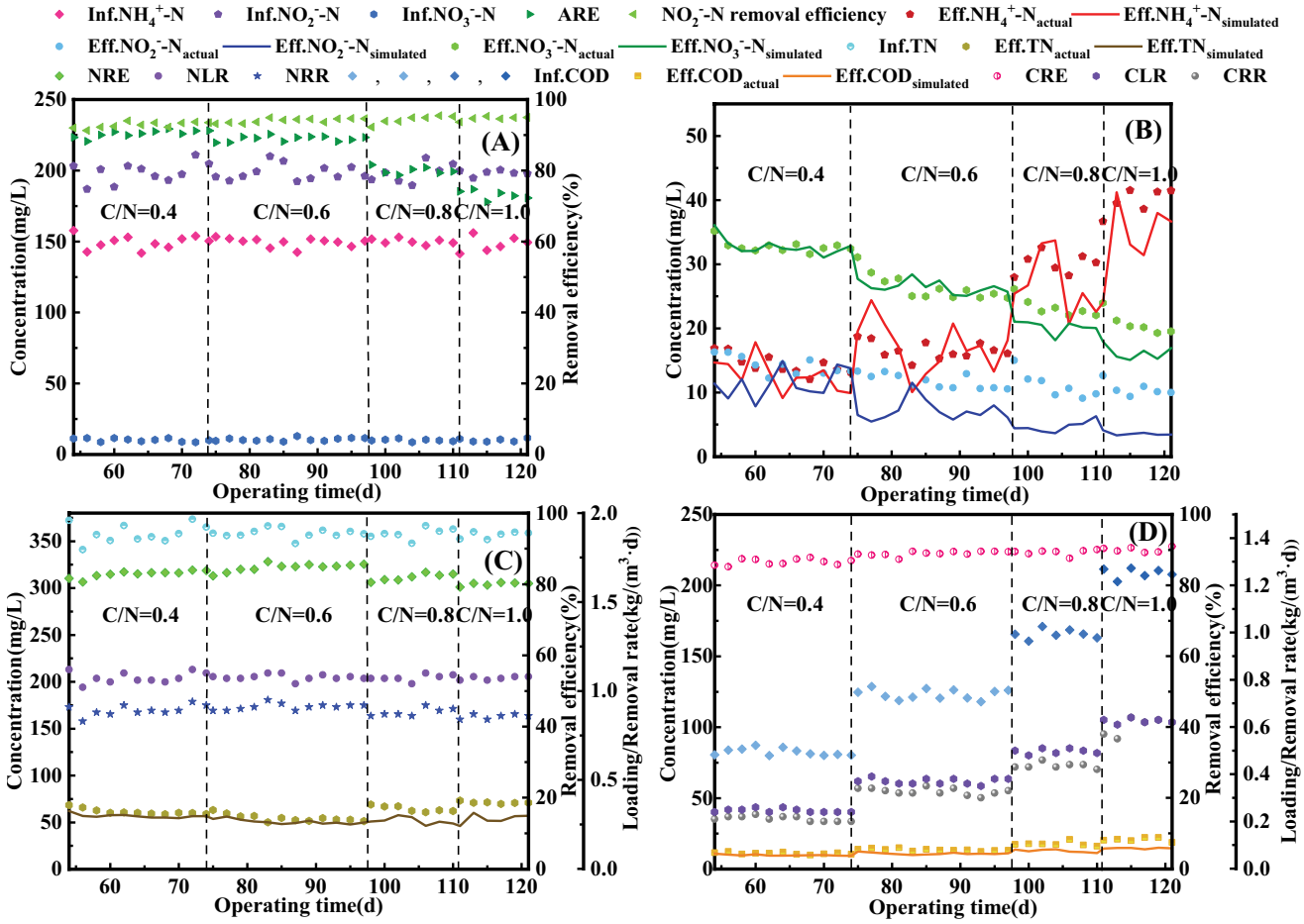

Fig. 5. The performance and simulation results of the SAD process at different C/N ratios. (A) NH_4^+–N, NO_2^-–N, and NO_3^-–N removal, (B) effluent NH_4^+–N, NO_2^-–N, and NO_3^-–N concentrations, (C) TN removal, and (D) COD removal.

Table 7
Simulated nitrogen and COD removal of the SAD process at different C/N ratios

Time (d)	Inf.COD (mg/L)	Inf.NH_4^+–N (mg/L)	Inf.NO_2^-N (mg/L)	Inf.NO_3^-N (mg/L)	C/N ratio	Eff.COD (mg/L)	Eff.NH_4^+–N (mg/L)	Eff.NO_2^-N (mg/L)	Eff.NO_3^-N (mg/L)	ARE (%)	NRE (%)	CRE (%)
1~31	62.34	105.0	198.0	9.8	0.3	9.44	10.67	13.01	35.07	92.89	83.58	84.86
32~62	83.12	105.0	198.0	9.8	0.4	9.8	12.72	10.46	31.79	91.52	84.64	88.21
63~93	103.90	105.0	198.0	9.8	0.5	10.24	15.51	8.5	28.9	89.66	85.21	90.14
94~124	124.68	105.0	198.0	9.8	0.6	10.74	18.97	7.09	26.36	87.35	85.35	91.39
125~155	145.46	105.0	198.0	9.8	0.7	11.27	22.97	6.07	24.08	84.69	85.15	92.25
156~186	166.24	105.0	198.0	9.8	0.8	11.83	27.32	5.32	21.98	81.78	84.73	92.88
187~217	187.02	105.0	198.0	9.8	0.9	12.43	31.92	4.75	20.03	78.72	84.15	93.35
218~248	207.80	105.0	198.0	9.8	1.0	13.08	36.69	4.28	18.19	75.54	83.46	93.71

Note: Values in the table are the average of each period.

effluent NO_2^-–N and NO_3^-–N concentrations showed the opposite pattems. The simulated effluent NO_2^-–N and NO_3^-–N concentration gradually decreased from 13.01 and 35.07 to 4.28 and 18.19 mg/L, respectively. This was attributed to the consumption of NO_2^-–N or NO_3^-–N by the DNB via heterotrophic denitrification. The simulated effluent COD concentration increased from 9.44 to 13.08 mg/L as the C/N ratio increased; the CRE increased from 84.86% to 93.71%.

The pattern for the simulated NRE was different. When the C/N ratio increased from 0.3 to 0.6, NRE increased from 83.58% to 85.35%; however, when the C/N ratio increased from 0.6 to 1.0, NRE decreased from 85.35% to 83.46%. Thus, the maximum NRE was obtained at a C/N ratio of 0.6 during the simulation, indicating that AnAOB and DNB had the optimal synergistic effect under this condition. The optimal C/N ratio of 0.6 was obtained through mathematical modeling. To verify the simulation data, four C/N ratios including the optimized simulated one (0.4, 0.6, 0.8, and 1.0) were used for experimental verification.

3.3.1.2. Experimental verification of process performance at different C/N ratios

The process performance of the SAD system at different influent C/N ratios is shown in Fig. 5. As the C/N ratio increased from 0.4 to 1.0, the ARE decreased from 90.38% to 73.11%, and NO_2^-–N removal efficiency remained high (94.85%), which was similar to the simulation results and consistent with the observed trend. The concentrations of NH_4^+–N and NO_3^-–N in the experimental effluent were close to the simulated data, and the observed trend was consistent (Fig. 5B). The experimental NO_2^-–N value was slightly higher than the simulated one, but the trend was the same. The NLR and NRR were maintained at high levels: 1.07 kg/(m^3·d) and 0.89 kg/(m^3·d), respectively (Fig. 5C). However, the NRE first increased and then decreased as the C/N ratio increased. The NRE attained its highest value of 84.74% at a C/N ratio of 0.6, which was close to the simulation value of 85.35%. Moreover, as the C/N ratio increased, the CLR and CRR increased in a phased manner from 0.25 kg/(m^3·d) and 0.20 kg/(m^3·d) to 0.63 kg/(m^3·d) and 0.60 kg/(m^3·d), respectively (Fig. 5D). During the entire process, CRE gradually increased from 86.60% to 90.05%, which was slightly lower than the simulated one (from 88.21% to 93.71%). Overall, the validity of the simulated data from the mathematical model was further confirmed through the experimental verification.

3.3.2. Influence of different C/N ratios on microbes during SAD process optimization

Functional bacteria (AerAOB, NOB, AnAOB, and DNB) at different C/N ratios were simulated (Fig. 6). Under the initial condition at each C/N ratio, the AnAOB concentration decreased. As the reactor continued to operate, AnAOB gradually adapted to the altered environment, and its growth rate gradually decreased as the C/N ratio increased. However, AnAOB was still the dominant microbial species; its concentration ranged from 4494–5104 mg MLSS/L. By contrast, the growth rate of DNB gradually increased as the

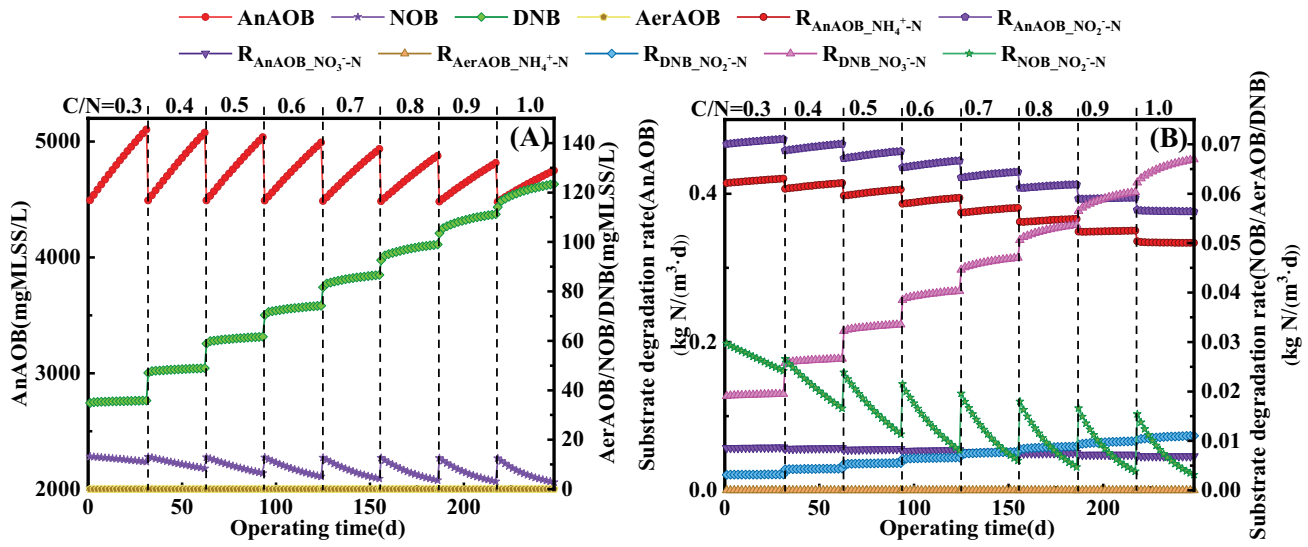

Fig. 6. Simulation of (A) the concentrations and (B) activity of functional bacteria at different C/N ratios.

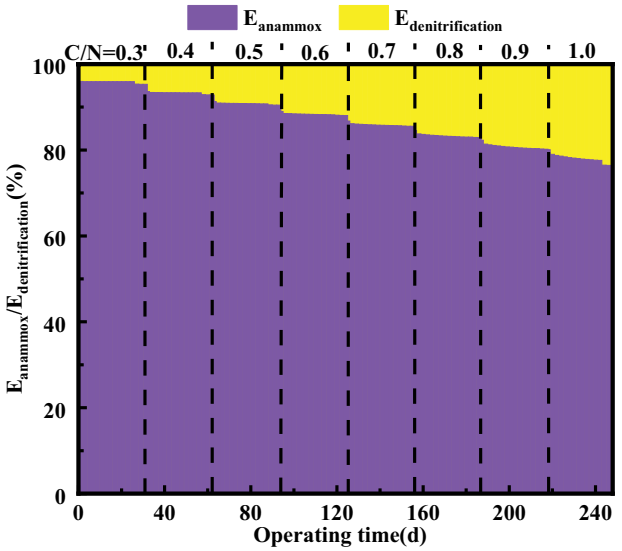

Fig. 7. Changes in $E_{anammox}$ and $E_{denitrification}$ at different C/N ratios

C/N ratio increased; its concentration gradually increased from 34.90 to 123.40 mg MLSS/L. The activity of AnAOB and DNB showed similar trends as the microbial concentrations at the same C/N ratio (Fig. 6B). AnAOB activity, as estimated by the degradation rates of NH_4^+–N and NO_2^-–N, decreased from 0.4142 and 0.4668 kg N/(m³·d) to 0.3336 and 0.3759 kg N/(m³·d), respectively. DNB activity increased as the C/N ratio increased, and the degradation rates of NO_2^-–N and NO_3^-–N increased from 0.0031 and 0.0191 kg N/(m³·d) to 0.0110 and 0.0669 kg N/(m³·d), respectively. These results reflected the gradual increase in the strength of competition for substrates and living space between AnAOB and DNB in the SAD system as the C/N ratio increased. Nevertheless, lower concentrations and activity of AerAOB and NOB could provide a better coupling environment for AnAOB and DNB.

3.3.3. Changes in the contribution rates of nitrogen removal at different C/N ratios

As the C/N ratio increased, $E_{anammox}$ gradually decreased (Fig. 7). The average $E_{anammox}$ was 95.81% at a C/N ratio of 0.3, and it decreased to 78.01% when the C/N ratio increased to 1.0. Conversely, $E_{denitrification}$ increased as the C/N ratio increased. The average $E_{denitrification}$ gradually increased from 4.19% at a C/N ratio of 0.3 to 21.99% at a C/N ratio of 1.0. This can be explained by the increase in the abundance of the carbon source, which increased DNB activity and their abundance in the reactor, thereby enhancing the denitrification process. Generally, AnAOB and DNB show synergy and competition in the coupling process. When the C/N ratio increased from 0.3 to 0.6, the NRE gradually increased, indicating that the synergistic effect of AnAOB and DNB was gradually enhanced. However, when the C/N ratio increased from 0.6 to 1.0, the NRE gradually decreased, indicating that the synergy gradually weakened, and competition gradually increased. These findings indicated that the optimal synergy was achieved at a C/N ratio of 0.6 when NRE achieved its maximum value. At this time, $E_{anammox}$ and $E_{denitrification}$ were 83.33% and 16.67%, respectively, indicating that the anammox process was the dominant pathway in the coupled system, which permits efficient and stable nitrogen removal.

4. Conclusions

SAD process start-up was initiated by adding an organic carbon source into the anammox system at a C/N ratio of 0.25. At the end of the start-up period, ARE, CRE, NRE, and NRR reached 93.43%, 82.22%, 82.99%, and 0.90 kg/(m³·d), respectively. The mathematical model of the SAD process

start-up was then established using AQUASIM software. The simulation of the process performance and functional microbes could accurately reflect the operational characteristics of the SAD system. Furthermore, the optimal C/N ratio for the SAD process was determined to be 0.6 through the mathematical simulation and experimental verification. The highest NRE (85.35%) and the greatest degree of synergy in the anammox process ($E_{anammox}$ of 83.13%) and denitrification process ($E_{denitrification}$ of 16.67%) in the coupling system were achieved at this C/N ratio. Overall, the established model can offer an effective way to optimize the SAD process, thereby providing the practical guidance of the SAD process in the wastewater treatment.

Acknowledgments

This work was financially supported by the Hebei Provincial Natural Science Fund Project (E2021402011) and the Project of Young Top Talents Program in Universities and Colleges of Hebei Province (BJ2019029).

References

[1] T. Lotti, R. Kleerebezem, C. Lubello, M.C.M. van Loosdrecht, Physiological and kinetic characterization of a suspended cell anammox culture, Water Res., 60 (2014) 1–14.
[2] M. Strous, J.J. Heijnen, J.G. Kuenen, M.S.M. Jetten, The sequencing batch reactor as a powerful tool for the study of slowly growing anaerobic ammonium-oxidizing microorganisms, Appl. Microbiol. Biotechnol., 50 (1998) 589–596.
[3] I. Zekker, M. Raudkivi, O. Artemchuk, E. Rikmann, H. Priks, M. Jaagura, T. Tenno, Mainstream-sidestream wastewater switching promotes anammox nitrogen removal rate in organic-rich, low-temperature streams, Environ. Technol., 42 (2021) 3073–3082.
[4] I. Zekker, G.D. Bhowmick, H. Priks, D. Nath, E. Rikmann, M. Jaagura, T. Tenno, K. Tamm, M.M. Ghangrekar, ANAMMOX-denitrification biomass in microbial fuel cell to enhance the electricity generation and nitrogen removal efficiency, Biodegradation, 31 (2020) 249–264.
[5] Z.Z. Wang, Y. Ji, L. Yan, Y. Yong, H. Zhang, P. Gao, S.M. Li, Simultaneous anammox and denitrification process shifted from the anammox process in response to C/N ratios: performance, sludge granulation, and microbial community, J. Biosci. Bioeng., 130 (2020) 319–326.
[6] Z.Z. Wang, P. Gao, L. Yan, D. Zhao, Y. Ji, H. Zhang, S.M. Li, Simultaneous nitritation, anammox, and denitrification (SNAD) process in a membrane bioreactor: start-up, optimization, and membrane fouling behavior, Desal. Water Treat., 194 (2020) 69–84.
[7] M. Takekawa, G. Park, S. Soda, M. Ike, Simultaneous anammox and denitrification (SAD) process in sequencing batch reactors, Bioresour. Technol., 174 (2014) 159–166.
[8] S.X. Sheng, B. Liu, X.Y. Hou, Z. Liang, X.B. Sun, L.F. Du, D.P. Wang, Effects of different carbon sources and C/N ratios on the simultaneous anammox and denitrification process, Int. Biodeterior. Biodegrad., 127 (2018) 26–34.
[9] F. Gao, J. Nan, S.N. Li, Y.R. Wang, Modeling and simulation of a biological process for treating different COD:N ratio wastewater using an extended ASM1 model, Chem. Eng. J., 332 (2018) 671–681.
[10] B.A.B. Zhen, T.B. Masashi, P.B. Giri, S.B. Satoshi, Z.A. Jiti, Q.A. Sen, I.B. Michihiko, Effects of the C/N ratio and bacterial populations on nitrogen removal in the simultaneous anammox and heterotrophic denitrification process: mathematic modeling and batch experiments, Chem. Eng. J., 280 (2015) 606–613.
[11] J.Y. Yang, J. Li, Z.M. Zheng, J. Du, J. Ma, W. Bian, W.X. Wang, Effect of organic compounds on the SAD and its mathematical simulation, J. Environ. Sci. (China), 38 (2018) 4516–4523.
[12] M. Azari, M. Lübken, M. Denecke, Simulation of simultaneous anammox and denitrification for kinetic and physiological characterization of microbial community in a granular biofilm system, Biochem. Eng. J., 9 (2017) 206–216.
[13] APHA, AWWA, WEF, Standard Methods for the Examination of Water and Wastewater, 21st ed., American Public Health Association, American Water Works Association, Water Environment Federation, Washington DC, USA, 2005.
[14] L. Gong, M. Huo, Q. Yang, J. Li, B. Ma, R. Zhu, S. Wang, Y. Peng, Performance of heterotrophic partial denitrification under feast-famine condition of electron donor: a case study using acetate as external carbon source, Bioresour. Technol., 133 (2013) 263–269.
[15] S. Milia, M. Perra, G. Tocco, A. Carucci, The start-up of an anammox reactor as the second step for the treatment of ammonium rich refinery (IGCC) wastewater with high C org/N ratio, Ecol. Eng., 106 (2017) 358–368.
[16] M. Kumar, J.-G. Lin, Co-existence of anammox and denitrification for simultaneous nitrogen and carbon removal—strategies and issues, J. Hazard. Mater., 178 (2010) 1–9.
[17] U. Wiesmann, Biological nitrogen removal from wastewater, Adv. Biochem. Eng./Biotechnol., 51 (1994) 113–154.
[18] J. Meng, J.L. Li, J.Z. Li, Z.B. Min, The effects of influent and operational conditions on nitrogen removal in an upflow microaerobic sludge blanket system: a model-based evaluation, Bioresour. Technol., 295 (2020) 122225, doi: 10.1016/j.biortech.2019.122225.
[19] B.J. Ni, A. Joss, Z. Yuan, Modeling nitrogen removal with partial nitritation and anammox in one floc-based sequencing batch reactor, Water Res., 67 (2014) 321–329.
[20] M. Strous, J.J. Heijnen, J.G. Kuenen, M.S.M. Jetten, The sequencing batch reactor as a powerful tool for the study of slowly growing anaerobic ammonium-oxidizing microorganisms, Appl. Microbiol. Biotechnol., 50 (1998) 589–596.
[21] X.D. Hao, J.J. Heijnen, M.C.M. van Loosdrecht, Sensitivity analysis of a biofilm model describing a one-phase completely autotrophic nitrogen removal (CANON) process, Biotechnol. Bioeng., 77 (2010) 266–277.
[22] W. Gujer, M. Henze, T. Mino, M.V. Loosdrecht, Activated sludge model No. 3, Water Sci. Technol., 39 (1999) 183–193.
[23] D. Kaelin, R. Manser, L. Rieger, J. Eugster, K. Rottermann, H. Siegrist, Extension of ASM3 for two-step nitrification and denitrification and its calibration and validation with batch tests and pilot scale data, Water Res., 43 (2009) 1680–1692.
[24] J. Meng, J.L. Li, J.Z. Li, J. Nan, M. Zheng, The effects of influent and operational conditions on nitrogen removal in an upflow microaerobic sludge blanket system: a model-based evaluation, Bioresour. Technol., 295 (2020) 122225, doi: 10.1016/j.biortech.2019.122225.